

# Photonic Barcodes Combining Branched Hybridization Chain Reaction for Multiplex Quantification of Bladder Cancer MicroRNAs

Xiaowei Wei, Zehan Cai, Lijun Cai, Yu Wang, Dagan Zhang,\* and Yefei Zhu\*

Bladder cancer is the most common malignant tumor of the urinary system with substantial therapy cost and mortality. Recently, quantification and multiplex detection of circulating microRNAs (miRNAs) from human serum has opened a new avenue for efficient diagnosis of bladder cancer. Herein, a novel multiplex platform is designed toward bladder cancer-related miRNAs detection by integrating photonic crystal (PhC) barcodes with the branched hybridization chain reaction (B-HCR). PhC barcodes possess constant characteristic reflection peaks originating from the highly ordered microstructure and thus exhibit vivid structural colors as the encoding elements. B-HCR is an isothermal enzyme-free amplification strategy on the basis of hybridization chain reaction (HCR), which presents a higher amplification efficiency. By integrating the vivid structural colors of PhC barcodes with the isothermal amplification of B-HCR, this platform shows an acceptable accuracy, reproducibility, and high sensitivity for multiplex detection of low-abundance miRNAs. Moreover, the results are consistent with conventional qRT-PCR in the serum specimens. Therefore, this platform may provide a new approach for the clinical diagnosis of bladder cancer.

with the higher sensitivity and better patient compliance for the diagnosis, prognosis and surveillance of bladder cancer due to the poor sensitivity of traditional cytology tests, especially for low grade tumors, and the high invasiveness of cystoscopy.<sup>[1,4]</sup> Recently, liquid biopsy ushers a new era of noninvasive cancer detection because it is capable of isolating a variety of cancer-related molecules for further detection, including circulating tumor cells, exosomes, cell-free proteins, peptides, and microRNAs (miRNAs).<sup>[5]</sup> Among them, circulating miRNAs have attracted the most scientific interest during the last decades as it has been proved to express aberrantly in several tumors including bladder cancer.<sup>[6–8]</sup> Thus, circulating miRNAs could serve as novel biomarkers for cancer detection and prognosis.<sup>[9–11]</sup> At present, there are many highly sensitive methods for miRNAs detection and signal amplification strategies,<sup>[12–14]</sup>

## 1. Introduction

Bladder cancer is a malignant urological disease, which brings the heavy physiological and economic burden to patients due to the high incidence rate, recurrence rate, and unsatisfactory screening methods.<sup>[1–3]</sup> Over the decades, the intensive investigation has focused on the developing of new screening methods

including hybridization chain reaction (HCR),<sup>[15,16]</sup> Polymerase Chain Reaction (PCR),<sup>[17]</sup> loop-mediated isothermal amplification (LAMP),<sup>[18]</sup> Rolling Circle Amplification (RCA),<sup>[19]</sup> and other novel schemes.<sup>[20–22]</sup> Notably, due to the cumbersome extraction and low expression abundance of miRNA in clinical specimen, HCR was been widely used in biosensing, bioimaging, and biomedicine, as a classic and efficient isothermal amplification molecular biotechnology, benefiting from the non-enzymatic, ultra-high sensitivity, and structural flexibility.<sup>[23,24]</sup> Branched hybridization chain reaction (B-HCR) is a non-linear amplification approach based on HCR.<sup>[25]</sup> The target sequences played the bridging role and the additional HCR circuits were initiated through the branching sequences. More branches were assembled in each round of the linear extension, thus improving the analytical sensitivity. Although B-HCR system increased the complexity of the sequence design, the recursive start of this control system was still a technical challenge, which requires us to continuously optimize the conditions to obtain better enhancement effect.<sup>[26,27]</sup> In addition, the traditional detection platforms could no longer meet the high specific requirement of the clinical disease diagnosis by detecting a single specimen at one time. Thus, it is urgent to develop a new platform with composite multiplex quantification as well as high sensitivity.

Herein, we proposed the photonic crystal (PhC) barcodes combined with B-HCR strategy to construct a multiplexed

X. Wei, Z. Cai, Y. Zhu  
Laboratory Medicine Center  
The Second Affiliated Hospital of Nanjing Medical University  
Nanjing 210011, China  
E-mail: zhuyf@njmu.edu.cn

L. Cai, Y. Wang  
State Key Laboratory of Bioelectronics  
School of Biological Science and Medical Engineering  
Southeast University  
Nanjing 210096, China

D. Zhang  
Department of Rheumatology and Immunology  
Institute of Translational Medicine  
The Affiliated Drum Tower Hospital of Nanjing University Medical School  
Nanjing 210008, China  
E-mail: zhang\_dagan@126.com

 The ORCID identification number(s) for the author(s) of this article can be found under <https://doi.org/10.1002/admi.202102515>.

DOI: 10.1002/admi.202102515

analysis system for bladder cancer-related miRNA detection. Up to now, an ocean of barcodes have been devised for multiplex detection, such as fluorescent particles, semiconductor quantum dots and PhC.<sup>[28–32]</sup> Among them, PhC barcodes stand out on account of the distinct merits including remarkable encoding stability, free of the fluorescent background or photobleaching.<sup>[33–38]</sup> To be specific, PhC barcodes can exhibit characteristic reflection peaks and vivid structural colors due to the photonic band gap (PBG) originating from their highly ordered alignment of nanoparticles.<sup>[39–43]</sup> Therefore, multiplexed detection could be easily realized by utilizing the different PhC barcodes embedded with the corresponding biomolecule probes as the encoding element, holding great clinical potential.

In this paper, we report a novel platform for the multiplex quantification of bladder cancer-related miRNAs by integrating the advantages of PhC barcodes and B-HCR (**Scheme 1**). The PhC barcodes were obtained through self-assembly of silica nanoparticles in microfluidic devices. The adequate surface area of these PhC barcodes benefited the immobilization of probe molecules. The target miRNAs could be captured by the probes, which initiated the cross-opening of H1 and H2, respectively, to form the DNA polymerized nanowires. Meanwhile, the extended region of H1 could be used as a branch to trigger the extension of H3 and H4, showing a higher fluorescence intensity. It was demonstrated that the sensitivity of this detection system in the complex media could reach the femtomolar level due to the combination of PhC barcodes and B-HCR. Furthermore, the results were consistent with qRT-PCR method which is commonly used in clinical laboratories. Therefore, this platform is expected to provide a promising platform for the multiplex quantification of the low-abundance miRNAs in bladder cancer diagnosis.

## 2. Results and Discussion

### 2.1. Preparation and Characterization of PhC Barcodes

In a typical experiment, PhC particles were fabricated from the self-assembly of silica nanoparticles in microfluidic droplets. First, silica nanoparticles were synthesized by Stöber method.<sup>[44–46]</sup> Then, the silica nanoparticles were dispersed in water and set as inner phase in the microfluidic device, where the disperse phase was sheered into droplets (Figure S1, Supporting Information). PhC particles were obtained after high-temperature calcination to improve the mechanism strength. Under natural light irradiation conditions, these particles exhibited vivid structural colors. Later, scanning electron microscopy (SEM) was utilized to observe the microstructure of the PhC barcodes. As shown in **Figure 1a–c**, the microstructure of the PhC barcodes showed the highly ordered hexagonal alignment, which provided a nanopatterned platform for biomolecule reaction and probes immobilization. Moreover, the highly ordered alignment of the nanoparticles contributed to the formation of PBG, resulting in the vivid structural colors. To be specific, light of a wavelength located within the band gap was unable to propagate and thus reflected from the surface of the PhC barcodes, thereby exhibiting the specific corresponding structural color and the distinctive reflection peaks.

Under normal incidence, the characteristic reflection peak position of the PhC barcodes can be calculated by Bragg's equation:<sup>[47,48]</sup>

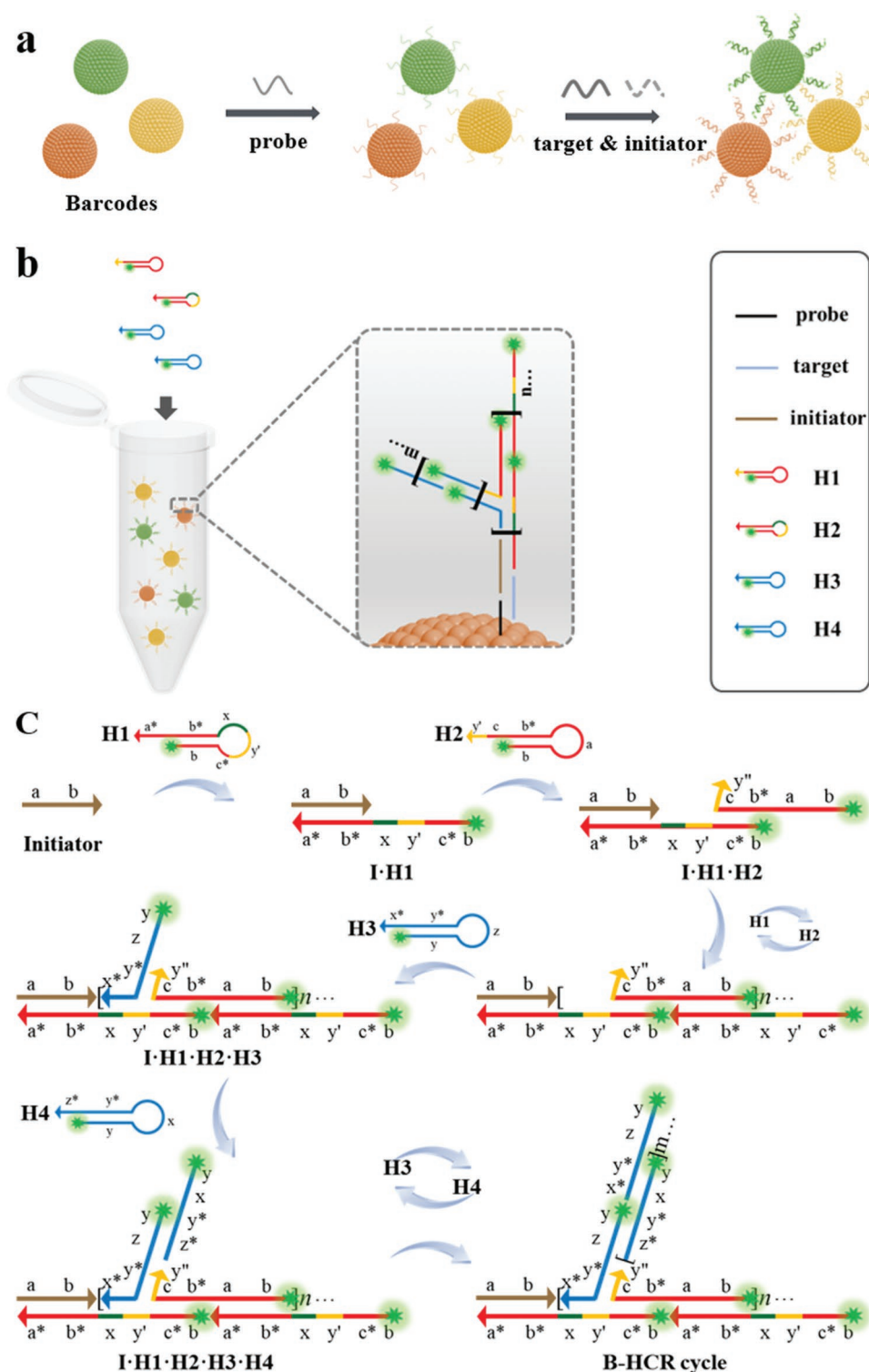
$$\lambda = 1.633dn_{\text{average}} \quad (1)$$

where  $\lambda$  is the peak wavelength,  $d$  is the center-to-center distance between two neighboring nanoparticles and  $n_{\text{average}}$  is the average refractive index of the barcodes. Therefore, a repertoire of PhC barcodes with different characteristic reflection peaks and the corresponding structural color could be obtained by changing the diameter of the silica nanoparticles (Figure 1d–f). Here, Stöber method was used to synthesize the silica nanoparticles. By adjusting the temperature of the reaction system, nanoparticles with different sizes could be prepared and further self-assembled to form the periodic ordered structures. Due to the difference spacing of nanoparticles, different characteristic reflectance spectra were generated as the multiple encoding elements (Figure 1g–i).

### 2.2. Establishment the Analysis Platform with PhC Barcode Combined with B-HCR

MiRNA in clinical specimens is often at trace level, which needs to be supplemented by signal amplification. Compared to enzyme-based rolling-circle amplification strategies in our previous work, HCR is a highly efficient isothermal amplification strategy due to the enzyme-free, simple operation. Therefore, PhC barcodes combined with HCR strategy may construct an ideal and highly efficient platform for the multiplex miRNA quantification. In this work, we designed a B-HCR approach by improving the branch section according to the mechanism of HCR. Different from classical HCR, B-HCR presents the stronger detection signal in the nonlinear amplification mode. To confirm the feasibility of the B-HCR strategy, the polymer formation was first detected by gel electrophoresis. In **Figure 2a**, band 1, 2, 3, and 4 indicated that the lengths of H1, H2, H3, and H4 were less than 50 bp, which was consistent with the sequence design length. Band 5 showed that initiator sequence (initiator, I) reacted with H1. Moreover, band 6 revealed that HCR reaction occurred when initiator sequence, H1 and H2 coexisted, thus proving the feasibility of HCR. Similarly, agarose gel electrophoresis was used to validate B-HCR reaction. As shown in **Figure 2b**, band 2 expressed that if only initiator sequence, H3 and H4 present, amplification reaction didn't work. While in band 3, initial sequence and H1, H2, H3, H4 participate in the B-HCR reaction. By comparing, it could be found that the products of band 3 were significantly more than band 1, indicating that B-HCR reaction extended based on HCR, thus resulting the backward movement of bands. On the contrary, band 4 showed that, in the absence of initiation sequence, H1, H2, H3, and H4 did not react with each other, whose hairpin structures remain stable.

Based on the design of B-HCR strategy, we established a detection platform combining PhC barcode with B-HCR, and analyzed the fluorescence intensity of the non-amplification, HCR method and B-HCR by comparison, as shown in **Figure 2c**. The results demonstrated that, benefit from the



**Scheme 1.** a) Schematic diagram of the multiplexed detection of miRNAs by PhC barcodes; b) schematic diagram of the signal amplification based on B-HCR strategy; c) schematic diagram of the sequence hybridization of B-HCR strategy.

spatial amplification effect of the branched chains, B-HCR achieved more efficient signal amplification based on the linear amplification of the classical HCR. Applied to the bioanalysis, the fluorescence signal intensity of B-HCR strategy

(Figure 2c-iii) was more significant compared with the classical HCR group (Figure 2c-ii) and the non-amplified group (Figure 2c-i), indicating the feasibility and detection efficiency of the multiplexed analysis platform.



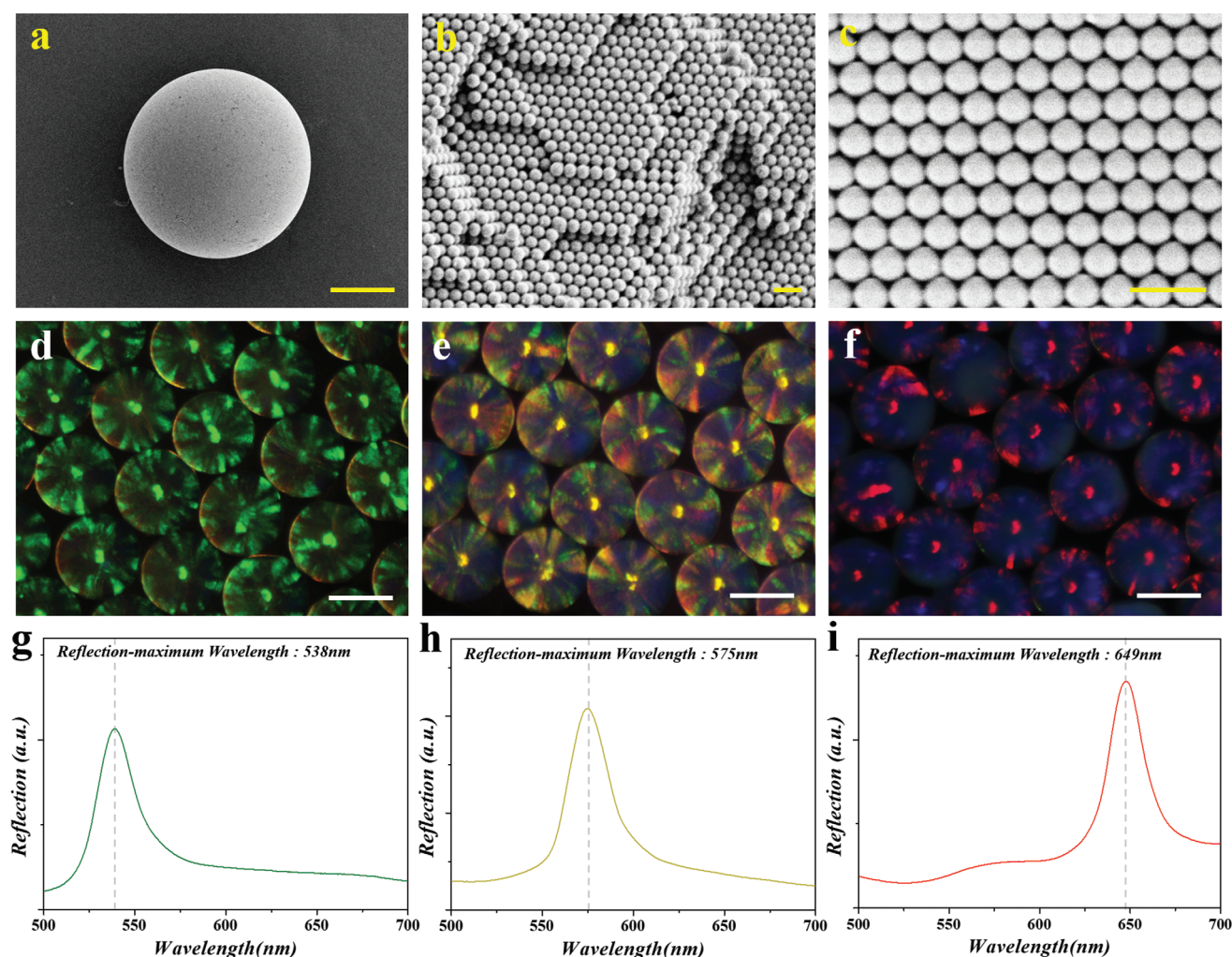


**Figure 1.** a) SEM image of the surface of PhC barcodes; scale bar is 50  $\mu\text{m}$ . b–c) The ordered hexagonal arrangement of monodisperse silica nanoparticles inside; scale bars are 50 nm. d–f) Reflection images of PhC barcodes with structural colors of green, yellow, and red, prepared from 244261 and 295 nm diameter nanoparticles, respectively. Scale bars are 200  $\mu\text{m}$ . g–i) The corresponding characteristic reflection peaks of PhC barcodes.

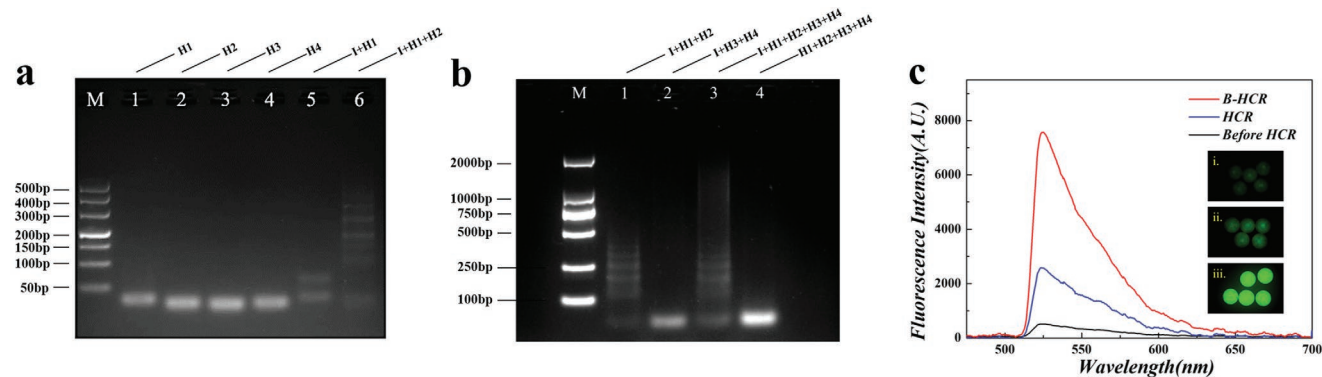


**Figure 2.** a) Gel electrophoretic map of HCR regimen. Agarose concentration was 3.5%; lane 1: 500 nm H1; lane 2: 500 nm H2; lane 3: 500 nm H3; lane 4: 500 nm H4; lane 5: 500 nm I + 500 nm H1; lane 6: 500 nm I + 500 nm H1 + 500 nm H2. b) Gel electrophoresis of B-HCR scheme. Agarose concentration was 2%; lane 1: 500 nm I + 500 nm H1 + 500 nm H2; lane 2: 500 nm I + 1  $\mu\text{m}$  H3 + 1  $\mu\text{m}$  H4; lane 3: 500 nm I + 500 nm H1 + 500 nm H2 + 1  $\mu\text{m}$  H3 + 1  $\mu\text{m}$  H4; lane 4: 500 nm H1 + 500 nm H2 + 1  $\mu\text{m}$  H3 + 1  $\mu\text{m}$  H4. c) The fluorescence spectrum and corresponding images of carboxy-fluorescein (FAM) decorated target miRNA and B-HCR products. Image i shows the fluorescent intensity of the conventional detection (target + H1); image ii shows the fluorescent intensity of the HCR (target + H1 + H2); image iii shows the fluorescent intensity of B-HCR (target + H1 + H2 + H3 + H4). The concentrations of probes and targets were selected from the working concentration (1  $\mu\text{M}$ ) indicated in the sequence synthesis instruction.

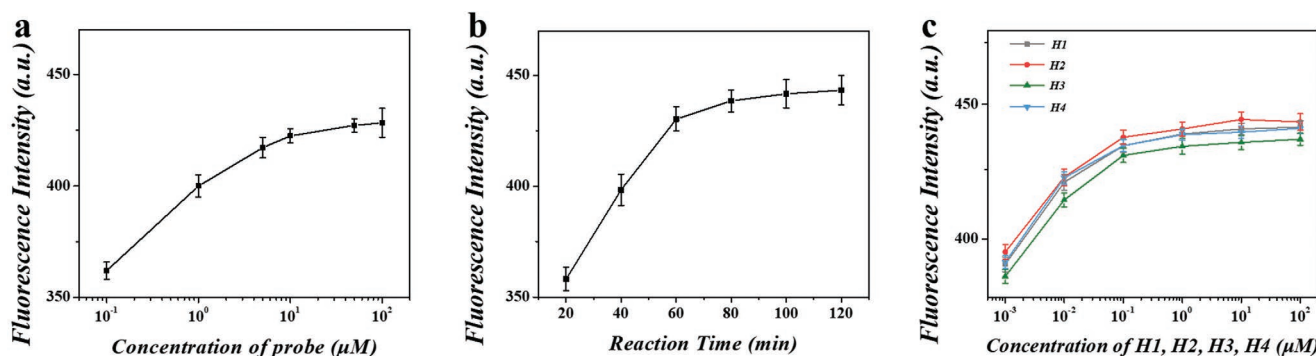


**Figure 3.** a) The relationship of fluorescence intensity with the concentration of probe. b) The relationship of fluorescence intensity with the B-HCR extension time. c) The relationship of fluorescence intensity and the concentration of  $\approx$ H1–H4.

### 2.3. Detection Condition Optimization

In this detection system, we combined PhC barcodes with B-HCR strategy, and explored the stability and potential of the quantitative platform under different experimental conditions. Considering the sensitivity of this platform, concentration of probes was explored and optimized. By incubating the barcodes with different concentrations of probes and then mixing it with saturated target miRNA-133a, we found that the fluorescence intensity of HCR-branched PhC barcodes gradually increased with the increasing of probe concentration, and tended to be stable when the probe concentration was over 0.1  $\mu\text{M}$  (Figure 3a). As a crucial parameter of signal amplification performance, B-HCR extension reacting time was also discussed. As shown in Figure 3b, the fluorescence intensity gradually increased and reached a stable level with the incubation time from 20 to 60 min. Contrastive analysis was conducted with and without target markers in the detection system (Figure S2, Supporting Information). The significant difference in fluorescence intensity ( $p < 0.001$ ) indicated the ideal sensitivity and specificity of this platform. In addition, we discussed the working concentration of the amplified hairpin sequence  $\approx$ H1–H4, and the results indicated that 0.1  $\mu\text{M}$  was the optimal concentration to participate in the B-HCR signal amplification strategy (Figure 3c).

Under these optimized conditions, the correlation between the miRNA concentration and fluorescence intensity was investigated. The results of the data showed that the fluorescence intensity of the PhC barcodes combined with B-HCR increased when the concentration of target miRNAs from  $10^{-5}$  to  $10^2$   $\mu\text{M}$ , and an ideal fitting correlation coefficient from  $10^{-4}$  to  $10^2$   $\mu\text{M}$  (Figure 4a–c). Moreover, the concentrations of target miRNAs in different reaction mediators, including serum and whole blood, were compared with those in PBS buffer. Considering the base detection values of target miRNAs in serum and whole blood specimens, we deduced them as the background interference. The results showed that the concentration-signal effect of miRNAs in serum was similar to that in PBS; however, the signal response performance of whole blood specimens may be reduced due to the complex matrix (Figure S3, Supporting Information). Distinguishing targets with the similar base sequences was a major challenge in miRNA multiplex detection. To further verify the specificity of this detection system,

we constructed the mutant sequences based on the target miRNAs. The results showed that the fluorescence intensity would significantly reduce even when the target sequence was mutated by a single base, which demonstrated the reliable specificity of this platform for the multiplex analysis of miRNAs (Figure 4d–f). In addition, we mixed the target sequence with the similar sequence (1 bm) in a ratio of 100:1 to compare with the pure target sequence. The detection result was close to the pure target sequence, which more effectively verified the anti-interference performance of this detection platform (Figure S4, Supporting Information).

### 2.4. Multiplexed Analysis of Bladder Cancer Related miRNAs based on PhC Barcode Combined with B-HCR

In this platform, the probe molecules were chemically coupled with the PhC microcarriers to specifically capture the target miRNAs, while the B-HCR amplification system was activated by the complementary initiator sequences. Among this process, the different molecular probes bind to the PhC barcodes with different structural colors to achieve the high sensitivity multiplexed detection of target miRNAs (Figure 5a). Here, PhC barcodes with the characteristic reflection peaks at 538 nm (green), 575 nm (yellow), and 649 nm (red) were used to simultaneously quantify the miRNA-200b, miRNAs-133a, and miRNA-143b, respectively. In the same reaction tube, these barcodes were modified with the corresponding probes to capture the miRNA targets, and then incubated in a mixture of H1, H2, H3, and H4. After B-HCR amplification, the microscope images manifested that fluorescence signal could be observed only for the barcodes coupled with the miRNA target (Figure 5b), while the fluorescence intensity could be measured by the fluorescence spectrometer for quantitative analysis of the target miRNAs (Figure 5c). In addition, PhC barcodes could be used to detect and distinguish multiple targets in the mixed samples (Figures S5 and S6, Supporting Information). These results indicated that the PhC barcodes combined with B-HCR were capable for multiplex quantification of miRNAs with an ideal specificity and anti-interference performance. Moreover, we discussed the reproducibility of PhC encoding microcarriers based on the encoding element, that is, the characteristic reflection peak wavelength, and the detection signal intensity.

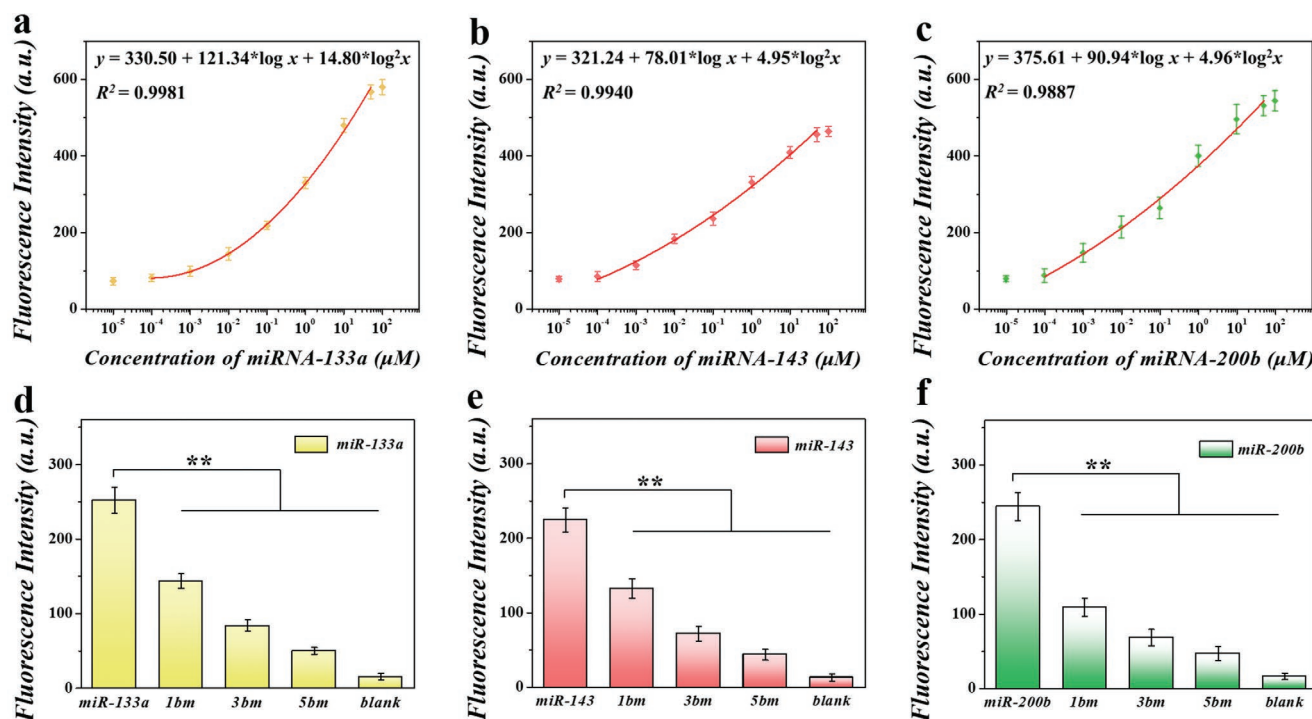


**Figure 4.** a–c) Curve-fitting analysis of the concentration of the target miRNAs and fluorescence intensity. d–f) Fluorescence intensity analysis of PhC barcodes encoding target sequences and base mutation sequences.

The concentration ( $10^{-1} \mu\text{M}$ ) with an acceptable response in the concentration-signal intensity fitting curve was selected as the analytical concentration, and the detection was repeated for 20 times. The results show that the structural color reflection spectrum of PhC barcodes and the signal intensity have the ideal encoding stability and reproducibility respectively (Table S1, Supporting Information).

## 2.5. Clinical Application of PhC Barcodes Combined with B-HCR

The PhC barcode combined with B-HCR was employed to conduct the multiplex detection of bladder cancer-associated miRNAs. We analyzed the serum specimen from bladder cancer patients and healthy control group, which were collected from the second Affiliated Hospital of Nanjing Medical University of China by standard venipuncture (Institutional Review Board protocol number [2020]-KY-003). Informed written consent was obtained from patients. The staging data of bladder cancer patients and the corresponding miRNA detection levels were presented in Table S2 and Table S3, Supporting Information, respectively. Blood specimen (5 mL) were collected from patients before surgery, and centrifuged at  $3000 \text{ r min}^{-1}$  for 10 min to separate the serum for detection. Then, the efficacy of the selected target miRNAs in the diagnosis of Bladder cancer was evaluated by receiver operator characteristic (ROC) curve (Figure 6a–c). The results showed that the areas under the curve (AUC) corresponding to miR-133a, miRNA-143, and miRNA-200b were 0.722, 0.647, and 0.782, respectively, indicating that these target markers had an acceptable prospect for the auxiliary diagnosis of bladder cancer based on this multiplexed analysis platform. Moreover, qRT-PCR, a widely used method

for miRNA detection in the clinical laboratories, was utilized to comparative analysis with this platform. With the concentration of target miRNAs as the x-axis, the fluorescence signal intensity and qRT-PCR cycle numbers were plotted as the double-y-axis curves. The results showed that the multiplexed quantification of miRNA based on PhC barcode combined with B-HCR strategy had a good consistency with the data distribution trend of qRT-PCR method (Figure 6d–f). In addition, the linear regression analysis based on PhC barcodes and qRT-PCR for the specimens indicated an ideal correlation (Figure S7, Supporting Information), which further confirmed the reliability and potential of PhC barcodes combined with B-HCR in the practical application.

## 3. Conclusion

In summary, we have developed a novel detection system based on PhC barcodes combining with B-HCR for multiplex quantification of bladder cancer related miRNAs. The highly ordered alignment of PhC particles not only ensured the encoding stability but also provided a nanopatterned reaction platform. Since PhC barcodes were encoded by the stable characteristic reflection peaks and B-HCR could be realized under the isothermal conditions without enzyme, low-abundance miRNAs could be quantified simultaneously with an acceptable accuracy and ideal repeatability. By taking advantages of PhC barcodes and B-HCR, the detection limit could reach to  $10^{-4} \mu\text{M}$  in the serum, a complex media. Furthermore, in the analysis of clinical specimens, the detection results were consistent with the common laboratory methods, which confirmed the accuracy of this platform. Therefore, PhC barcodes combined with



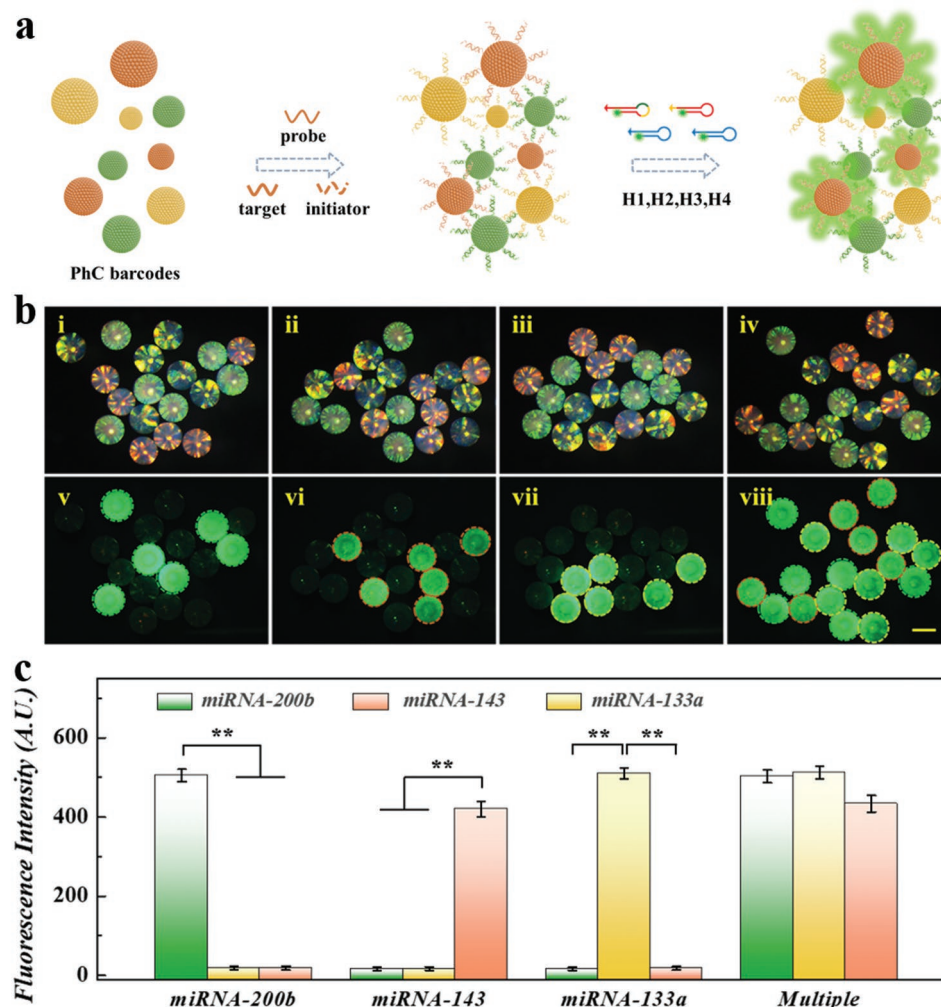


**Figure 5.** a) Schematic diagram of the specificity of PhC barcodes with B-HCR for multiplex miRNA detection; b) optical microscopy images (i–iv) and fluorescence images (v–viii) of PhC barcodes with B-HCR; scale bar is 200  $\mu\text{m}$ . c) The fluorescence intensity statistics of PhC barcodes combined with B-HCR.

B-HCR may provide a promising diagnostic strategy for multiplex quantification of low-abundance miRNA in the diagnosis of bladder cancer.

## 4. Experimental Section

**Materials:** 2-Morpholinoethanesulfonic acid (MES) was bought from AMRESCO LLC (Solon, USA). 1-ethyl-3-(3-dimethylaminopropyl) carbodiimide (EDC) and N-hydroxy succinimide (NHS) were purchased from Aladdin Reagent Co., Ltd. All oligonucleotides were synthesized from Nanjing Ruizhen Biotechnology Co. Ltd (detailed sequence information in Table S4, Supporting Information). Deionized water was obtained by Millipore Milli-Q system (Millipore, Bedford, MA) (with the electric resistance  $>18.25\text{ M}\Omega$ ) and used in all experiments. All the chemical reagents were of the optimal grade. The electrophoresis buffer consisted of Tris (40 mM), acetic acid (20 mM), EDTA- $\text{Na}_2$  (2 mM), and  $(\text{CH}_3\text{COO})_2\text{Mg}$  (TAE-Mg).

**Instruments:** The mechanical syringe pumps and the constant pressure pumps were provided by Suzhou Co-microfluidics Technology Co., Ltd. The microfluidic device used for generating silica colloidal crystal particles was self-made by this research group. All reactions were

finished in a constant temperature shaker (Thermomixer comfort 5355, Eppendorf, Germany). The microstructures of the PhC barcodes were characterized by scanning electron microscope (SEM, S-300N, Hitachi, Japan). The photographs of PhC barcodes were taken by the optical microscope (BX51, Olympus, Japan) equipped with a CCD camera (MP5.0, Media Cybernetics Evolution). The reflection spectra of the barcodes were recorded by the same microscope fitted with a fiberoptic spectrometer (HR2000, Ocean Optics, USA). The fluorescence intensity was measured by a fluorescence microscope (BX53, Olympus, Japan). The fluorescence images of multiplex detection were snapped by a stereoscopic microscope (Olympus, SZX16) equipped with the camera under halogen lamp (Olympus, LG-PS2) and mercury lamp (Olympus, U-RFL-T).

**Preparation of PhC Barcodes:** According to the previous work of the research group,<sup>[49–51]</sup> PhC encoding microcarriers were prepared by microfluidic droplet cutting method. Three different diameters (244, 261, and 295 nm) of monodisperse silica nanoparticles were used as the dispersed phase for generation of PhC barcodes. The dispersed phase was water suspension containing 20% W/V monodisperse silica nanoparticles at a fluid velocity of  $0.5\text{ mL h}^{-1}$ , which was cut into droplets by silicon oil (50 cSt) via the microfluidic device at a fluid velocity of  $3.0\text{ mL h}^{-1}$ . Then, the droplets were collected in methyl silicone oil (500 cSt) stood to evaporate to form highly ordered colloidal

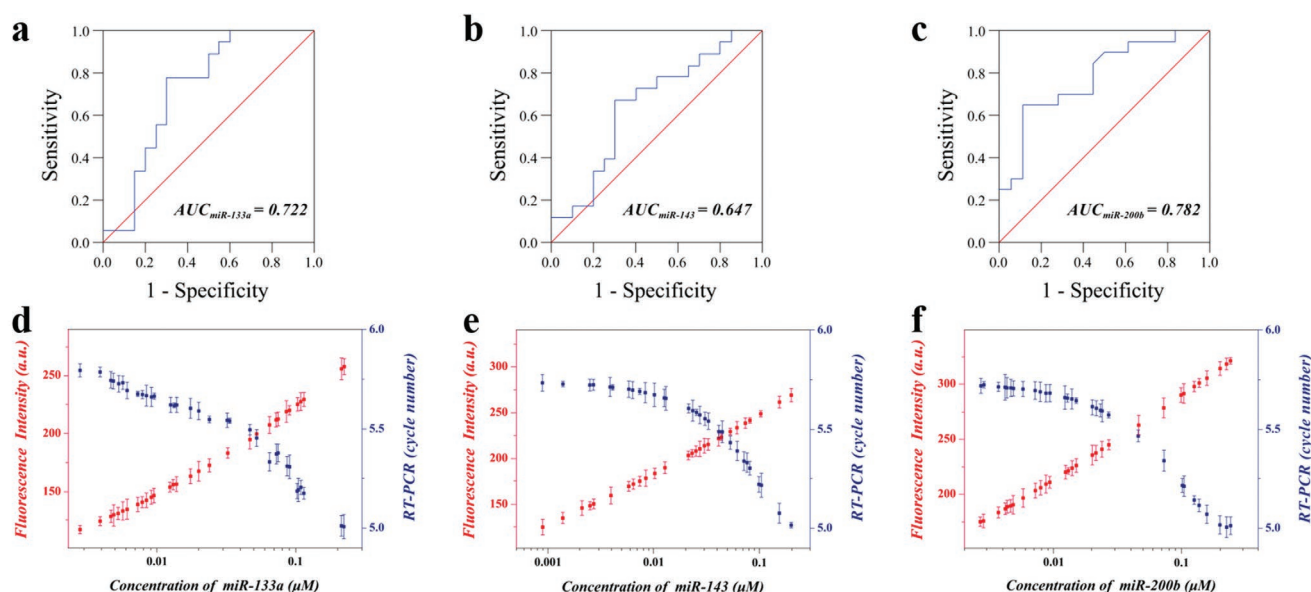


**Figure 6.** a–c) ROC curves of multiplex detection of bladder cancer-related miRNAs by PhC barcode combined with B-HCR. d–f) The detection results of PhC barcodes are compared with qRT-PCR method in the clinical specimens. The number of repetitions for each clinical specimen is 3. The error bar is the standard deviation.

crystal beads at 65 °C for 12 h. Then, hexane was utilized to remove the remaining silicon oil on the surface for five times. Finally, the silica colloidal crystals were calcined at 800 °C for 6 h to improve the mechanical strength.

**Probe Immobilization:** First, PhC barcodes were immersed in 0.1% NaOH (W/V) for 15 min. After being washed with PBS for three times, PhC barcodes were aminated for 6 h in an ethanol suspension containing 2% APTES (W/V) in constant oscillator at 37 °C. After washing three times with the anhydrous ethanol, PhC barcodes were added into DMSO solution of 10% succinic anhydride (W/V) for 12 h at 37 °C, with the amino group transformed into carboxyl group, and the unreacted part washed with DMSO for three times. In MES buffer (pH 6.0), carboxyl groups on the surface of PhC barcodes were activated by EDC and NHS and incubated at 37 °C for 1 h, which reacted with the amino modified probe molecules to achieve chemical coupling. Finally, the unreacted probes were washed with PBS buffer solution.

**Branched HCR Reaction:** The target miRNAs and the initiators were added successively into MES buffer and kept at 37 °C for 1 h in the thermostatic oscillator. After that, the remaining sequences were removed by deionized water. Then, the hairpin sequences of H1, H2, H3, and H4 were heated to 95 °C for 2 min. The PhC barcode was oscillated at 37 °C for 2 h with the mixture of H1, H2, H3, and H4. Here, the FAM-labeled H3 and H4 sequences acted as the branch, triggering the B-HCR to exhibit the prominent fluorescence intensity.

**Gel Electrophoresis Analysis:** Integrating DNA technology design tools (<http://eu.idtdna.com/pages/scitools>) was used for the feasibility analysis of the formation of hairpin structure and primer hybridization (Figure S8, Supporting Information). Then, hairpin sequence was heated to 95 °C for 2 min, then cooled naturally to the room temperature for use. The 3% agarose gel (w/w) or 2% (w/w) agarose gel was electrophoresis analyzed in 1×TAE buffer. The electrophoresis was performed at a constant potential of 75V for 10 h after loading 2 µL of each sample into the lanes.

**Statistical Analysis:** All of the analytical data were processed by Origin Lab 2019b and SPSS Statistics 26. Independent-samples *t* test was used to analyze the fluorescence signal intensity between detection groups. In clinical cases, Student's *t*-test was used for continuous variable (age, years), while Chi-square test for categorical variables between cases and controls. Pearson correlation was used to evaluate the consistency of

laboratory detection methods. The efficacy of biomarker analysis based on this platform for clinical diagnosis was evaluated by the area under the ROC curve.

## Supporting Information

Supporting Information is available from the Wiley Online Library or from the author.

## Acknowledgements

X.W. and Z.C. contributed equally to this work. This work was supported by the “333 project” High-level Talent Cultivation Foundation of Jiangsu (Grant no. BRA2018086), the Social Development Foundation of Clinical Frontier Technology of Jiangsu (Grant no. BE2017763), the Second Affiliated Hospital of Nanjing Medical University Medical Development and Support Fund, and the Natural Science Foundation of Anhui province (Grant No. 2008085QH365).

## Conflict of Interest

The authors declare no conflict of interest.

## Author Contributions

Y.F.Z. and D.G.Z. conceived the idea and designed the experiment; X.W.W., Z.H.C., and Y.W. conducted experiments and data analysis; X.W.W., L.J.C., and D.G.Z. wrote the manuscript.

## Data Availability Statement

Research data are not shared.



## Keywords

bladder cancer, branched hybridization chain reaction, miRNA, multiplex detection, photonic barcodes

Received: December 21, 2021

Revised: March 12, 2022

Published online: June 7, 2022

- [1] C. Berdik, *Nature* **2017**, 551, S34.
- [2] A. Lenis, P. Lec, K. Chamie, M. Mshs, *JAMA, J. Am. Med. Assoc.* **2020**, 324, 1980.
- [3] G. Xu, M. Lai, R. Wilson, A. Glidle, J. Reboud, J. Cooper, *Microsyst. Nanoeng.* **2019**, 5, 37.
- [4] D. Kaufman, W. Shipley, A. Feldman, *Lancet*. **2009**, 374, 239.
- [5] M. Di, J. Bartlett, Y. Cheng, M. Pasic, G. Yousef, *Mol. Cancer* **2017**, 16, 80.
- [6] L. Selth, W. Tilley, L. Butler, *Endocr. Relat. Cancer* **2012**, 19, R99.
- [7] H. Yoshino, N. Seki, T. Itesako, T. Chiyomaru, M. Nakagawa, H. Enokida, *Nat. Rev. Urol.* **2013**, 10, 396.
- [8] H. Dong, J. Lei, L. Ding, Y. Wen, H. Ju, X. Zhang, *Chem. Rev.* **2013**, 113, 6207.
- [9] Y. Uchida, T. Chiyomaru, H. Enokida, K. Kawakami, S. Tatarano, K. Kawahara, K. Nishiyama, N. Seki, M. Nakagawa, *Urol. Oncol.* **2013**, 31, 115.
- [10] S. Noguchi, T. Mori, Y. Hoshino, K. Maruo, N. Yamada, Y. Kitade, T. Naoe, Y. Akao, *Cancer Lett.* **2011**, 307, 211.
- [11] C. Kohler, O. Bryk, S. Meier, K. Lang, P. Rozynek, T. Bruning, H. Kafferlein, T. Bruning, H. Kafferlein, *Biochem. Biophys. Res. Commun.* **2013**, 438, 48.
- [12] W. Usuba, F. Urabe, Y. Yamamoto, J. Matsuzaki, H. Sasaki, M. Ichikawa, S. Takizawa, Y. Aoki, S. Niida, K. Kato, S. Egawa, T. Chikaraishi, H. Fujimoto, T. Ochiya, *Cancer Sci.* **2019**, 110, 408.
- [13] Y. Ma, S. Gamagedara, *Biomarkers Med.* **2015**, 9, 845.
- [14] I. Lodewijk, M. Dueñas, C. Rubio, E. Munera-Maravilla, C. Segovia, A. Bernardini, A. Teixeira, J. Paramio, C. Suárez-Cabrera, *Int. J. Mol. Sci.* **2018**, 19, 2514.
- [15] S. Bi, S. Yue, S. Zhang, *Chem. Soc. Rev.* **2017**, 46, 4281.
- [16] Y. Wei, W. Zhou, X. Li, Y. Chai, R. Yuan, Y. Xiang, *Biosens. Bioelectron.* **2016**, 77, 416.
- [17] P. Androvic, L. Valhrach, J. Elling, R. Sjoback, M. Kubista, *Nucleic Acids Res.* **2017**, 45, e144.
- [18] X. Zhang, S. Lowe, J. Gooding, *Biosens. Bioelectron.* **2014**, 61, 491.
- [19] M. Ali, F. Li, Z. Zhang, K. Zhang, D. Kang, J. Ankrum, X. Le, W. Zhao, *Chem. Soc. Rev.* **2014**, 43, 3324.
- [20] K. Ren, Y. Xu, Y. Liu, M. Yang, H. Ju, *ACS. Nano* **2018**, 12, 263.
- [21] L. Wang, R. Deng, J. Li, *Chem. Sci.* **2015**, 6, 6777.
- [22] S. Zhang, J. Chen, J. Liu, H. Pyles, D. Baker, C. Chen, Y. De, *Adv. Mater.* **2020**, 33, e1905784.
- [23] T. Zhao, H. Zhang, H. Tang, J. Jiang, *Talanta* **2017**, 175, 121.
- [24] Y. Xu, H. Wang, C. Luan, F. Fu, B. Chen, H. Liu, Y. Zhao, *Adv. Funct. Mater.* **2018**, 28, 1704458.
- [25] L. Liu, J. Liu, H. Wu, X. Wang, R. Yu, J. Jiang, *Anal. Chem.* **2018**, 90, 1502.
- [26] F. Xuan, I. Hsing, *J. Am. Chem. Soc.* **2014**, 136, 9810.
- [27] H. Chandran, A. Rangnekar, G. Shetty, E. Schultes, J. Reif, T. Labeau, *Biotechnol. J.* **2013**, 8, 221.
- [28] Y. Zhao, H. Shum, H. Chen, L. Adams, Z. Gu, D. Weitz, *J. Am. Chem. Soc.* **2011**, 133, 8790.
- [29] Y. Zhao, X. Zhao, Z. Gu, *Adv. Funct. Mater.* **2010**, 20, 2970.
- [30] S. Lee, J. Kim, Y. Kim, S. Kim, *Sci. Adv.* **2018**, 4, eaat8276.
- [31] M. Yang, Y. Liu, X. Jiang, *Chem. Soc. Rev.* **2019**, 48, 850.
- [32] H. Xu, J. Zhang, Y. Xu, H. Wang, F. Fu, Q. Xu, Y. Cai, *Sens. Actuators B. Chem.* **2018**, 255, 2690.
- [33] J. Ji, W. Lu, Y. Zhu, H. Jin, Y. Yao, H. Zhang, Y. Zhao, *ACS Sens.* **2019**, 4, 1384.
- [34] Y. Xu, X. Zhang, C. Luan, H. Wang, B. Chen, Y. Zhao, *Biosens. Bioelectron.* **2017**, 87, 264.
- [35] F. Bian, J. Wu, H. Wang, L. Sun, C. Shao, Y. Wang, Z. Li, X. Wang, Y. Zhao, *Small* **2018**, 14, 1803551.
- [36] D. Zhang, F. Bian, L. Cai, T. Wang, T. Kong, Y. Zhao, *Biosens. Bioelectron.* **2019**, 143, 111629.
- [37] Y. Wang, L. Shang, F. Bian, X. Zhang, S. Wang, M. Zhou, Y. Zhao, *Small* **2019**, 15, 1900056.
- [38] F. Bian, L. Sun, L. Cai, Y. Wang, Y. Zhao, S. Wang, M. Zhou, *Biosens. Bioelectron.* **2019**, 133, 199.
- [39] Y. Xu, H. Wang, C. Luan, Y. Liu, B. Chen, Y. Zhao, *Biosens. Bioelectron.* **2018**, 100, 404.
- [40] F. Zheng, Y. Cheng, J. Wang, J. Lu, B. Zhang, Y. Zhao, Z. Gu, *Adv. Mater.* **2014**, 26, 7333.
- [41] X. Zhang, Y. Wang, J. Chi, Y. Zhao, *Research* **2020**, 2020, 1.
- [42] L. Cai, H. Wang, Y. Yu, F. Bian, Y. Wang, K. Shi, F. Ye, Y. Zhao, *Natl. Sci. Rev.* **2020**, 7, 644.
- [43] Y. Shang, Z. Chen, Z. Zhang, Y. Yang, Y. Zhao, *Bio-Des. Manuf.* **2020**, 3, 266.
- [44] Y. Liu, Y. Wang, Y. Wang, Y. Shu, H. Tan, Y. Zhao, *Bioact. Mater.* **2020**, 5, 917.
- [45] J. Hou, M. Li, Y. Song, *Angew. Chem. Int. Ed. Engl.* **2018**, 57, 2544.
- [46] Y. Zhang, A. Khademhosseini, *Science* **2017**, 356.
- [47] S. Park, Y. Xia, *Langmuir* **1999**, 15, 266.
- [48] Z. Gu, S. Kubo, W. Qian, Y. Einaga, D. Tryk, A. Fujishima, O. Sato, *Langmuir* **2001**, 17, 6751.
- [49] Y. Zhao, X. Zhao, C. Sun, J. Li, R. Zhu, Z. Gu, *Anal. Chem.* **2008**, 80, 1598.
- [50] L. Shang, Y. Cheng, Y. Zhao, *Chem. Rev.* **2017**, 117, 7964.
- [51] Y. Yu, Q. Wang, C. Wang, L. Shang, *Eng. Regen.* **2021**, 2, 96.